Energy 255 (2022) 124419

Contents lists available at ScienceDirect

Energy

journal homepage: www.elsevier.com/locate/energy

Thermo-economic analysis of an oxygen production plant powered by an innovative energy recovery system

José Ramón Serrano, Francisco José Arnau, Luis Miguel García-Cuevas*, Fabio Alberto Gutiérrez

CMT – Motores Térmicos. Universitat Politècnica de València, Camino de Vera s/n, Valencia, 46022, Valencia, Spain

ARTICLE INFO

Article history:
Received 22 November 2021
Received in revised form
4 May 2022
Accepted 30 May 2022
Available online 14 June 2022

Keywords:
Mixed ioninc-electronic conducting membrane
Oxy-fuel
O_2 production
Turbochargers
Thermo-economic analysis

ABSTRACT

Oxy-fuel combustion is considered an attractive alternative to reduce pollutant emissions, which uses high-purity oxygen mixed instead of air for combustion processes. However, purchasing large amounts of high-purity oxygen may be unprofitable for certain industrial sectors, discouraging its implementation. Considering this, the potential of an oxygen production cycle for factories using oxy-fuel combustion is studied by performing a thermo-economic analysis where high-purity oxygen, electricity, and natural gas prices are considered. Oxygen is produced by membrane means, where mixed ionic-electronic conducting membranes are used, which require high temperatures and pressure gradients to work properly. A set of turbochargers is implemented, chosen by scaling an off-the-shelf model, what introduces an innovative way of waste energy recovering for improving the performance of the cycle. The whole cycle is powered by waste heat from high temperature flue gases, and it is sized for a ceramic manufacturing factory. In this work, two cases are analysed, differentiated by considering additional heating and the vacuum generation method in the oxygen line. The first case exhibits smaller production levels, although better profitability (31 €t^{-1}), whereas the second case displays higher production levels and production costs (33 €t^{-1}). Both cases are competitive concerning the average price of high-purity oxygen, supposing an average of 50 €t^{-1} in wholesale markets, proving the potential of the proposed alternative for oxygen production.

1. Introduction

According to a report by the International Energy Agency [1], industrial processes accounted for 37% of the total global final energy use in 2018, with direct emissions of 8.5 Gt of CO_2 and 21.76 Mt of NO_x in 2015, representing 20% of the worldwide human-made emissions [2]. This energy is often required in high-temperature flows due to the demand of some industries in their processes: as high as 1450 °C in cement kilns or even 2000 °C in some ceramic factories. These high temperatures are commonly reached by burning fossil fuels, leading to significant CO_2 and NO_x emissions. In this context, oxy-fuel combustion is an attractive alternative to these plants to reduce polluting gases production, which consists of using high-purity oxygen instead of air during the required combustion process. The main benefits provided by this combustion type are:

- Avoid NO_x emissions due to the low content of N_2 in the process gases.
- Less flue-gases compared with air-fired combustion because the removal of nitrogen. This leads to a reduction of heat losses and, consequently, an increase in energy efficiency.
- Enables an easy separation of CO_2 from water vapour in the flue gases, using the difference in condensation temperature. This leads to more carbon capture opportunities.
- Higher combustion temperatures, because of higher oxygen concentrations, resulting in better efficiency of the process using the same fuel.
- High potential to be integrated with large industrial facilities as power or cement plants, where higher combustion temperatures could improve the efficiency in this type of processes [3].

Some applications and studies of oxy-combustion are found in the literature in fields as diverse as internal combustion engines

* Corresponding author.
E-mail address: luiga12@mot.upv.es (L.M. García-Cuevas).

https://doi.org/10.1016/j.energy.2022.124419

[4–7], power plants [8–10] and industrial processes [11–13]. In all these studies, reducing emissions and CO_2 capture are shown as their main benefits.

However, high-purity oxygen purchasing may be too expensive to some industry sectors due to transportation and storage costs, and the increasing demand due to industrial growth. The latter has caused, for example, an increase of 65% in the price in the United States in 20 years [14], and 24.4% due to economic changes associated to the COVID-19 pandemic. This market behaviour discourages oxy-fuel combustion applications in some industrial sectors and has motivated the research and implementation of self-production of oxygen in different contexts.

Nonetheless, the most extended and feasible method to produce oxygen, cryogenic air separation (CAS), does not exhibit a profitable behaviour during operation in many applications, as shown in the works of Escudero et al. [12], Cau et al. [15] or Xiong et al. [16], where energy penalties up to 6% are reported due to the integration of the air separation system in systems such as power plants. According to realistic economic trends analysed by Escudero et al. [12], CAS integration in industrial contexts is expected to be a possible alternative in the mid-term. Nevertheless, considerable financial risks are expected, as explained by Cau et al. [15]. In CAS, air components are separated according to their different boiling temperatures. According to the review performed by Wu et al. [17], several cryogenic plants are producing up to 150 t d^{-1} of O_2 (99.5% purity). However, CAS commercial units have low Second Law efficiencies ranging between 15% and 24% [18], where the electric power consumption is in the range of 160 kWh t^{-1} to 270 kWh t^{-1} [19]. In these units, 85% of the energy is used in the air compression and its distillation, being a highly-energy intensive process [20].

Considering this, although there are some advantages gained by applying oxy-fuel combustion, the thermo-economic penalties when cryogenic air separation is implemented have encouraged the study of alternative air separation systems, as the studies performed by Habib et al. [19]. In this context, most of the researchers related to oxy-fuel combustion are working in novel options for air separation, where three different technologies could be highlighted: pressure and temperature swing adsorption, chemical looping air separation (CLAS), and membrane separation [17].

Pressure swing adsorption consists of the separation of air components where N_2 is adsorbed in the surface of a material, generating an oxygen-enriched stream [21]. To separate gases, the material must have a preferential adsorption for N_2, which depends on pressure: high pressure must increase the amount of N_2 that is adhered to the material while low pressure decrease the adsorption amount to regenerate the material, creating a pressure cycle [17,22]. This technology is applied for small and medium productions, including the paper industry and medical applications, according to the NZ Institute of Chemistry [23]. The main difficulty to be solved to increase the installation sizes is the limited adsorption capacity that leads to a decrease in the O_2 production when higher flow rates are required [17].

On the other hand, the chemical looping air method consists of two interconnected reactors that use a carrier for oxygen transportation. In the first reactor, the oxygen carrier is exposed to atmospheric air, where an oxidation process occurs, thus generating an oxygen-depleted flow. Then, the carrier releases the oxygen in the fuel reactor, where a typical combustion process is performed [17]. It is a promising technology where some thermodynamic assessments have found an energy requirement lower than 4–5 times when compared with cryogenic methods [24,25]. However, this has been done only in laboratory-scale experiments and small pilot plants, being a method that requires further research and development, especially about oxygen carriers applicable in an extended range of temperatures [17].

Additionally, there are polymeric and ion transport membranes (ITM). Polymeric membranes base their operation on the different O_2 and N_2 diffusion rates through a membrane with a pressure gradient. Most membrane materials are more permeable to oxygen than to nitrogen due to differences in molecule sizes. Nevertheless, the production of high-purity oxygen is difficult because some N_2 always permeates through the membrane, resulting in oxygen-enriched air around 40% of O_2 rather than pure O_2. Nonetheless, when higher oxygen purity is demanded, two stages of separation could be applied, as shown in the reviews by Wu et al. [17] and Smith and Klosek [22].

Finally, ITM are membranes where oxygen ions are transported from the high-oxygen concentration or feed side to the low-oxygen concentration or permeate side [17]. In this type of membranes, O_2 molecules are adsorbed on an electrically conducting coating located over the surface of the membrane, where they are dissociated to form oxygen ions [17]. Generally, these membranes are composed of a type of dense ceramic compound with a particular crystal lattice structure, often called mixed oxygen ionic and electronic conducting (MIEC) materials [17,26]. In MIEC materials, oxygen ions can diffuse via the lattice vacancies or interstitial sites under the driving force of the oxygen chemical potential gradient across the membranes. MIEC membranes offer a permeation selectivity for oxygen of 100%, with a lower energy consumption than cryogenic distillation technology and less capital investment [26,27]. Among all the different MIEC membranes, $Ba_{0.5}Sr_{0.5}Co_{0.8}Fe_{0.2}O_{3-\delta}$ (BSCF) is one of the most popular materials implemented in high purity oxygen production because of its high permeation, performing a stable operation while the operating temperature is above 850 °C, according to Wu et al. [17], Zhu and Yang [26] and Arratibel Plazaola et al. [27].

MIEC membranes for air separation are a technology with high potential for commercialisation in the following years. There are studies of oxygen production by MIEC membrane means for applications as power plants that exhibit better economic performance and an efficiency improvement of up to 5% compared with cryogenic methods [28–30]. One of the leading organisation in creating membranes for air separation on a commercial scale, Air Products & Chemicals, has been working with different companies and institutes on this. They have been drawing up a multiphase plan considering a technical feasibility phase (Phase I with prototypes that generate high purity oxygen in a 0.1 TPD rate) to a commercial scale where a 2000 TPD production could be achieved [26]. In one of the latest reports from Air Products, Anderson et al. [31] exhibited the construction and operation of a test unit with a production capacity of 100 TPD and smaller-scale experiments that demonstrate the continued oxygen production for 15000 h. Also, Praxair can be highlighted as another organisation whose contributions are generating advances in generating a commercial-scale unit of air separation membranes [32]. They have reported patents of MIEC membranes development, applied in chemical and electric power applications [33,34]. With the above said, there are efforts to create the first commercial-scale units in the next few years that can compete in terms of energy consumption and production with CAS, where works in mechanical strength and density of membrane area per volume are topics that need improvements for practical applications [35].

Meanwhile, certain conditions must be reached to produce adequate O_2 flows in MIEC membranes. Zhu et al. [36] studied oxygen permeation through dense mixed-conducting perovskite ceramic membranes (BSCFO) under different conditions of temperature and feed pressure. It was found that elevated feed pressures increase oxygen permeation flux and temperatures as high as 900 °C are beneficial to oxygen recovery. Also, Li et al. [14] studied different models of oxygen transport through MIEC using different

materials and applications. Temperatures between 700 °C and 1000 °C are needed and considerable pressure gradients between feed and permeate sides are required. Given this, different scenarios of oxygen production can be obtained as variables as pressure gradients and temperatures in O_2 production cycles varied during its operation.

The interest in oxy-fuel combustion processes and oxygen production by means of MIEC membranes is demonstrated in all these published works. Nonetheless, as far as the authors of this manuscript know, there is no previously published literature in which off-design conditions of an oxygen production cycle for oxy-fuel combustion applications is studied. Additionally, the authors have not found literature where controllable variables such as turbomachine speeds or valve openings are modified to obtain different oxygen production levels for industrial applications.

Hence, the novelty of the present manuscript is the thermoeconomic analysis of a proposed oxygen production cycle performing in a wide range of operation. Also, to evaluate off-design conditions whose production is expected to be used in oxy-combustion processes within a ceramic-production facility. This cycle uses a MIEC membrane of BSFC material, whose waste heat of the flue gases is recovered to heat up and pressurise the MIEC feed air. In order to analyse off-design conditions, a parametric study is performed, varying controllable variables of the cycle such as turbomachine speeds and valve openings. The assessment of each operating point is performed in terms of oxygen production, energy consumption, and operational costs where current prices of high-purity oxygen, electricity, and natural gas are considered. The performance of the cycle is then compared with other oxygen production alternatives, and it is computed for a wide range of operating conditions.

Additionally, to rise the air pressure at the membrane inlet, a set of turbochargers are implemented to exploit the available energy from the outlet membrane gases, obtained after separating N_2 from the air. These turbochargers are chosen to rely on an off the shelf model commonly used in the automotive industry, which were scaled depending on the thermodynamic conditions (pressure and temperature) in which they operate. Two different cases are analysed, whose differences concern in the heat addition and driving energy of the vacuum pump in the oxygen line. On that basis, the main objectives of this study are mentioned as follows:

- Design and optimise two cases of a cycle of O_2 production by means of MIEC membranes powered by waste heat of flue gases of an industrial cycle and commercial off-the-shelf radial turbochargers, finding the critical elements from the point of view of the performance of the cycles.
- Assess the behaviour of the cycle from a thermoeconomical perspective in off-design conditions, using performance indicators such as O_2 mass flow (kg s^{-1}), production cost per mass of oxygen produced (€t^{-1}) and amount of O_2 per consumed energy (kg kW^{-1} h^{-1}).
- Assess the operative feasibility of the proposed cycles in terms of direct costs of operation, comparing against typical purchase costs found in O_2 wholesale markets (50 €t^{-1}).

2. Process description

The proposed oxygen production cycle cases are shown in Fig. 1 and Fig. 2. The current configuration has been established after an iterative process considering an oxygen production of 0.12 kg s^{-1}, driving 0.65 kg s^{-1} to 0.75 kg s^{-1} of air at atmospheric conditions and pursuing an inlet membrane pressure around 900 kPa. The cycle starts driving atmospheric air flow (25 °C, 100 kPa) through three initial intercooled compression stages (C1, C2, C3) coupled with expansion stages (T1, T2, T3), forming turbocharger systems. Also, an electric compressor is implemented to start the operation of the whole system. Then, the air flows into a set of heat exchangers to obtain thermal energy and recover energy from other parts of the cycle.

One of these heat exchangers contributes energy to the air flow by using flue gases from a furnace used to manufacture ceramic products (HE4 in Case 1 and HE3 in Case 2). Typically, the furnace produces a mass flow of 0.27 kg s^{-1} composed of CO_2 and H_2O steam, products of combustion processes. The temperature of this flow could be higher than 1000 °C, for which it is exploited to recover its thermal energy and drive the cycle by increasing the air temperature. In addition, a heater could be added to increase air temperature, generating two different cases depending on the presence of extra heat addition.

The air enters to a three-end MIEC membrane where oxygen is separated from the air. An oxygen-depleted flow (mainly N_2) is produced, where its remaining energy is recovered at two heat exchangers and in the set of turbines initially mentioned. On the other hand, the oxygen flow is cooled by going through two heat exchangers used to heat the air, and, finally, its temperature is reduced in a cooler before the vacuum pump to enhance its performance. This vacuum pump in the oxygen line could be driven electrically or by implementing a turbocharger, locating its turbine between high and medium pressure stages (T2 and T3), generating two options to be analysed.

Therefore, two different cases are studied, considering the possible combinations of the mentioned alternatives of heat addition or type of driving energy in the vacuum pump in the oxygen line:

Case 1: No heat addition/electric compressor at O_2 line. There is limited availability in thermal energy due to the absence of a heater to increase the temperature in the air flow and the high dependence on the conditions (mass flow and temperature) of the flue gases coming from the furnace. Therefore, vacuum generation in the oxygen line takes place using an electric compressor, exploiting the available enthalpy in the oxygen-depleted flow solely to increase the pressure in the air flow. Consequently, this alternative possesses a higher efficiency in the vacuum generation at the O_2 line than in Case 2.
Case 2: Heat addition/Turbocharging at O_2. A heater is added at the end of the heat exchangers stages. This heater increases the air temperature to 1000 °C, which is a typical value for MIEC membranes, by burning part of the produced O_2 with natural gas. Thus, the oxygen-depleted flow has more available energy. For this reason, a turbocharger is implemented for vacuum generation in the oxygen line, whose expansion stage is located between the high and medium pressure turbines (T3 and T2) to power up the compressor.

Therefore, there is control upon the inlet temperature at the membrane, improving its permeability. Nevertheless, there is a decrease in the vacuum generation efficiency due to the turbocharger use and the mass flow disequilibrium between both turbomachines (C0 and T0). The latter might cause an increase in the electric energy consumption of the high-pressure electric compressor, which could overcome the reduction of electric energy consumption caused by the removal of an electric compressor in the oxygen line. The vacuum pressure in the oxygen line is controlled by using a wastegate that varies the mass flow across T0, regulating the available energy in the turbine and, thus, the compressor power and the vacuum pressure in the last instance.

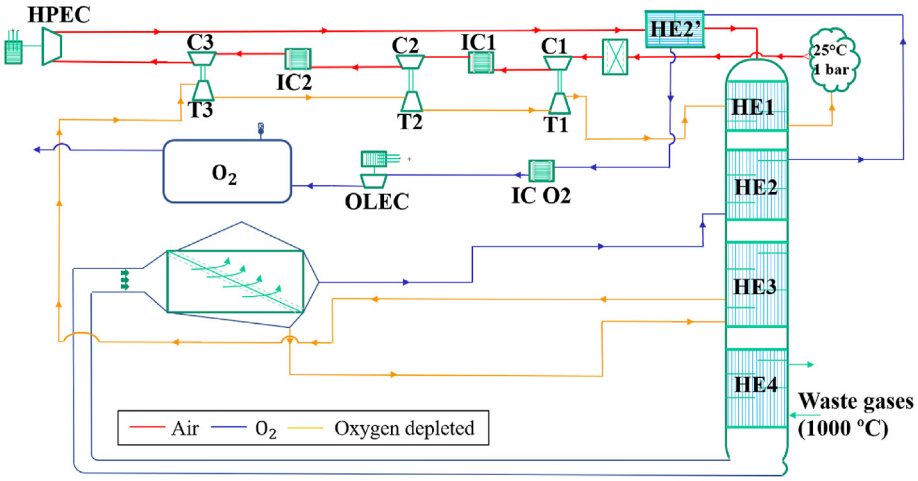

Fig. 1. Oxygen production cycle scheme for Case 1.

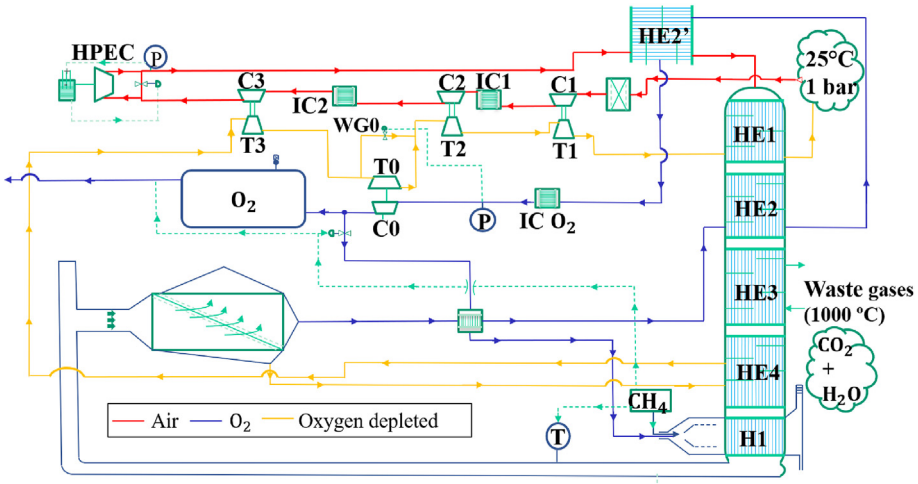

Fig. 2. Oxygen production cycle scheme for Case 2.

3. Method description

The cycle modelling was carried out using VEMOD [37], which is a computational tool developed at I·U·I CMT – Motores Térmicos originally aimed at 0D/1D modelling of thermo-and fluid dynamic processes in engines, but it is flexible to simulate independent elements such as turbochargers, coolers, pipes, heat exchangers, membranes, simple electric systems and control units. Moreover, VEMOD performs transient simulations, which enable the calculation start and stop conditions and determine resonant and unstable operation points.

Additionally, there is a set of assumptions and restrictions to be considered, to simplify the calculations and limit the performance evaluation performed.

3.1. Modelling

VEMOD solves Euler's fluid dynamics equations in 1D inside ducts using a finite-volume approach. The equations are solved using a MUSCL method, including heat transfer and friction effects using source terms obtained from correlations such as Colebrook-White's equation for Darcy's friction factor. Several elements are solved in 0D, such as the heat exchangers and the MIEC membrane: continuity and energy conservation equations are used, including source terms due to heat transfer or species permeation. In addition, oxygen production in the MIEC membrane is also determined as is described by Catalán-Martínez et al. [38], where simplified equations are given for 1D modelling.

The turbochargers are solved as actuator disks connected to equivalent 1D ducts, introducing momentum and energy sources and sinks from characteristic curves map data. They take into account also friction losses and heat transfer effects, as described in the works by Serrano et al. [39–42]. The turbine and compressor maps are extrapolated and interpolated as described in the works by Serrano et al. [43], Payri et al. [44], and Galindo et al. [45,46].

Additionally, it is known that for transient and pulsating conditions, shaft inertia of the turbochargers has a notable influence in the performance of both turbine and compressor as it is shown by Park et al. [47]. However, the influence of shaft inertia is not considered due the steady-state approach in this study.

3.2. Assumptions and simplifications

The following assumptions were taken into consideration to simplify the study:

- Isothermal flow inside the MIEC membrane as it is assumed in models found in the literature, which are validated using CFD [38] and experimental data [48,49] with accurate results.
- Pressure losses in the air line of 10 kPa for each heat exchanger.
- Heat exchanger effectiveness remain constant: there are no detailed specifications of heat exchangers in this preliminary design stage.
- Energy consumption of auxiliary components (cooler pumps, electrical and electronic devices) is not considered in this study.
- An additional cost of production of 18 €t^{-1} for each calculated point is considered estimating an installation cost of 570000 €. This cost is estimated after consulting several developers of this type of facilities and includes all the elements, the manufacturing, installation and labor costs. It supposes an average O_2 production of 100 g s^{-1} during a facility lifetime of 10 years, which is equivalent to the average O_2 consumption of the ceramic factory for which this facility has been sized.
- The heater in Case 2 is modelled considering a 85% efficiency, which considers heat losses and combustion efficiency. The air is heated with the gas products of burning part of the produced O_2 with natural gas (considered mainly CH_4). These gases leave the heater with a temperature difference of 10 °C with the temperature of the inlet air.

3.3. Components design and selection

The component design and selection uses reference conditions of air and oxygen mass flows through the whole cycle. Initially, the cycle is supposed to move 0.65 kg s^{-1} of air with a vacuum pressure of 40 kPa for Case 1 and 0.70 kg s^{-1} and a vacuum pressure of 35 kPa for Case 2.

The turbochargers used in the cycle were chosen taking as reference a typical commercial off-the-shelf (COTS) component from the automotive industry. Each turbomachine is scaled depending on the inlet temperature and pressure and flow capacity, pursuing a point of operation with high efficiency. The election of COTS turbocharger as a base lies in the high availability of this type of components, facilitating the purchase of replacement parts in case of wearing and maintenance, besides its competitive price.

The turbocharger taken as reference consists of a radial compressor with a wheel diameter of 40 mm, a maximum corrected mass flow of 0.14 kg s^{-1} and a maximum corrected speed of 229 000 rpm. It is driven by a radial variable nozzle turbine which has a wheel diameter of 37.5 mm, a maximum reduced mass flow of 12.16 kg s^{-1} $K^{0.5}$ MPa^{-1} and a maximum reduced speed of 112.2 Hz $K^{-0.5}$, whereas the shaft has a diameter of 6 mm.

The scaling process consists of keeping constant the non-dimensional mass flow and speed to maintain the similarity in the turbomachines, allowing the correct scalability. These non-dimensional groups are calculated using Equation (1) and Equation (2):

$$\hat{m} = \frac{\dot{m}\sqrt{\gamma \cdot R \cdot T_{1,t}}}{D^2 \cdot p_{1,t} \cdot \gamma} \tag{1}$$

$$\hat{N} = \frac{N \cdot D}{\sqrt{\gamma \cdot R \cdot T_{1,t}}} \tag{2}$$

where $\hat{m}$ is the non-dimensional mass flow, $\dot{m}$ is the mass flow, γ is the ratio of heat capacities, R is the gas constant, $T_{1,t}$ is the total temperature at the inlet of the turbomachine, D is the wheel diameter, $p_{1,t}$ is the total pressure at the inlet of the turbomachine, $\hat{N}$ is the non-dimensional rotational speed and N is the rotational speed.

Additionally, adiabatic efficiencies in each operation point of a scaled turbomachine remain constant as the exact Mach, Reynolds and dimensionless velocity triangles are assumed to be kept almost identical to the originals. Therefore, the adiabatic maps of each turbomachine are obtained to calculate real efficiencies considering heat and friction losses, which depend on several geometric variables of the turbomachine that are changed due to the applied scale.

Therefore, heat transfer and friction losses are calculated by considering the scale dimensions, where coefficients and areas of heat transfer between turbomachine components and the turbomachine itself with the environment are recalculated with the value of the scale. In contrast, linear values as diameters or lengths are determined by using the square root of the mentioned scale.

Concerning the efficiencies of the heat exchangers, special attention is given to HE3 for Case 1 and HE4 for Case 2, because of the coupling between the temperature increase in the air flow and the available energy in the expansion stages. In addition, the effectiveness of the other heat exchangers are set at 80%, considering the following restrictions:

- Avoid outlet temperatures at electric compressors higher than 200 °C, to prevent failures in the operation of these turbomachines, as their wheels are generally made of aluminium.
- Limit the effectiveness of the heat exchangers below values which could not be technically viable for the installation (greater than 90%).
- Maximise oxygen production.

Compressor sizes are selected such that the operation points in steady conditions have the best efficiency and a surge margin as wide as possible. Similarly, turbine sizes purse the best possible coupling with their respective compressors and the stator nozzle positions are selected using an optimisation process where the oxygen flow is maximised.

Regarding the membrane area, a higher area is expected in Case 1 to compensate for the lower amount of available energy at the membrane inlet. In this sense, a parametric study is performed, considering the produced oxygen and its associated costs, where a constant air mass flow driven by the compressor is assumed for each case, controlled by the high-pressure electric compressor (HPEC) speed.

3.4. Performance evaluation and analysis

A set of parameters were varied to generate operative maps as follows:

- High-pressure electric compressor (HPEC) speed.
- O_2 line electric compressor speed (OLEC) (in Case 1).
- Wastegate valve opening (in Case 2).

Three indicators were considered for the analysis of the maps: gross production, produced mass per unit of energy consumed (E (kg/kWh)), and O_2 production cost (C (€/t)). These indicators were used to evaluate the different variants of the cycle that were proposed from three different perspectives: gross production, economic and energetic.

The following prices in Table 1 for natural gas and electricity are used, considering several prices available in the current energy

market in Spain, not taking into account the transient price spikes during the 2021–2022 period.

For Case 1, the produced mass per energy (E) and O_2 cost (C) are calculated as stated in Equation (3) and Equation (4):

$$E(\text{kg/kWh}) = \frac{\dot{m}_{O_2}(\text{kg s}^{-1})}{\dot{W}_{HPEC}(\text{kW}) + \dot{W}_{OLEC}(\text{kW})} \cdot \frac{3600\ \text{s}}{1\ \text{h}} \tag{3}$$

$$C(€/\text{t}) = \frac{(\dot{W}_{HPEC}(\text{kWe}) + \dot{W}_{OLEC}(\text{kWe})) \cdot AEP}{\dot{m}_{O_2}(\text{kg s}^{-1})} \cdot \frac{1\ \text{h}}{3600\ \text{s}} \cdot \frac{1000\ \text{kg}}{1\ \text{t}} \tag{4}$$

On the other hand, the same indicators are calculated as proposed in Equation (5) and Equation (6):

$$E(\text{kg/kWh}) = \frac{\dot{m}_{O_2}(\text{kg s}^{-1})}{\dot{W}_{HPEC}(\text{kWe}) + \dot{Q}_h(\text{kWth})} \cdot \frac{3600\ \text{s}}{1\ \text{h}} \tag{5}$$

$$C(€/\text{t}) = \frac{\dot{W}_{HPEC}(\text{kWe}) \cdot AEP \cdot \frac{1\ \text{h}}{3600\ \text{s}} + \dot{m}_{NG}(\text{kg s}^{-1}) \cdot ANP \cdot CF}{\dot{m}_{O_2}(\text{kg s}^{-1})} \cdot \frac{1000\ \text{kg}}{1\ \text{t}} \tag{6}$$

4. Components selection

The selection of constructive variables as turbomachines and membrane sizes, turbine nozzle positions and effectiveness of critical heat exchangers is performed in this section considering the reference conditions given in subsection 3.3. A safe distance from surge line in the compressors case is kept when turbochargers sizes are selected, while the oxygen production and cost are considered for membrane size and heat exchanger effectiveness.

4.1. Turbocharger scaling

The following scaling values are selected concerning to compressor and turbine reference sizes, as shown in Table 2 for both cases:

For these scaling values, peak efficiency values that range between 60% and 70% for both types of turbomachines are obtained, and a cautious distance from the surge line in the case of the compressors is kept. Performance and efficiency maps of the scaled compressors are found in Appendix A.

4.2. Critical heat exchanger

4.2.1. Case 1

An increase in the effectiveness of this heat exchanger produces an increase in the oxygen mass flow because there is a higher temperature at the inlet of the membrane as shown in Fig. 3a. However, this increase in HE3 effectiveness decreases the available energy in the expansion stages, requiring an increment in the electric energy consumption by the HPEC.

Considering this, a value of 55% in this efficiency is selected, where a minimum value in the cost per production of oxygen can be found, as Fig. 3b shows, preserving an acceptable oxygen mass flow. As conclusion, an improvement in the heat transfer of this heat exchanger does not imply an enhancement in the global performance of the cycle.

Table 1
Current average prices of natural gas and electricity in Spanish market.

Average natural gas price (ANP)	0.026 €/kWh
Average electricity price (AEP)	0.100 €/kWh
Conversion factor for natural gas (CF)	13.89 kW h kg^{-1}

Table 2
Turbocharging scaling.

Case	Turbocharger	Compressor	Turbine
1	Low pressure	9	9
	Medium pressure	4	4
	High pressure	3	4
2	Low pressure	15	20
	Medium pressure	7	9
	High pressure	3	4
	O_2 line	4	4

4.2.2. Case 2

Net oxygen production increases almost linearly as the heat transfer in HE4 grows, as shown in Fig. 4a. This can be explained considering a decrease in gross production as the efficiency is rising. However, this also leads to a reduction in the heat that should be added in the heater, whose combustion process is performed using part of the produced oxygen, which finally conducts to a net oxygen production that increases with the efficiency of this particular heat exchanger.

Likewise, regarding cost per produced oxygen, whose behaviour is depicted in Fig. 4b. Higher efficiency in HE4 causes an increase in electrical energy consumption due to a reduction in the available energy in the expansion stages, increasing the electric compressor work. Nonetheless, this is compensated with a decrease in natural gas consumption in the heater, causing a reduction in the cost per produced oxygen. In this case, an efficiency value of 70% is selected, considering technical issues with higher values of efficiency as size, cost, and maintenance expenses.

4.3. Membrane area

A higher membrane area in the cycle allows an increase in oxygen production. Fig. 5a exhibits the oxygen production depending on the membrane area for Case 1, where an asymptotic behaviour is shown. There is not a considerable increment in oxygen production from 30 m^2 onwards. This performance is due to the decreased available energy in the expansion stages. The oxygen production grows, subtracting oxygen-depleted mass flow due to constant air mass flow, reducing the available energy through the turbines. This reduction in oxygen-depleted mass flow causes an increase in HPEC consumption. For this reason, a 30 m^2 is selected for this case. The latter is an effect that could also be perceived in Fig. 5b, where there

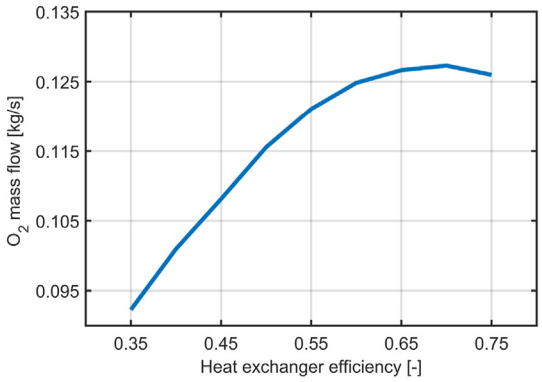

(a) Oxygen mass flow as a function of HE3 efficiency in Case 1.

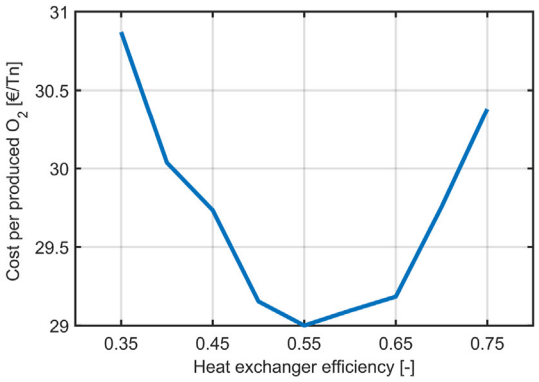

(b) Cost per produced oxygen variation respect to HE3 efficiency in Case 1.

Fig. 3. Oxygen production as a function of HE3 efficiency in Case 1.

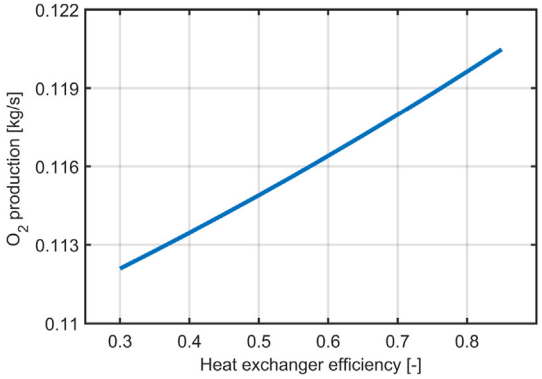

(a) Oxygen mass flow as a function of HE3 Efficiency in Case 2.

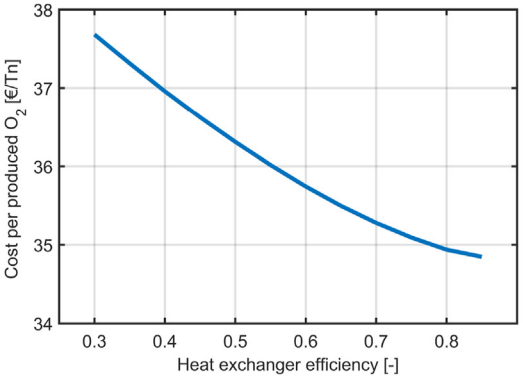

(b) Cost per produced oxygen variation respect to HE3 efficiency in Case 2.

Fig. 4. Oxygen production as a function of HE3 efficiency in Case 2.

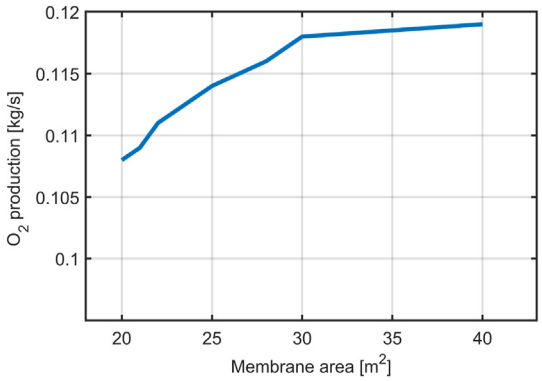

(a) Oxygen production variation respect to membrane area for Case 1.

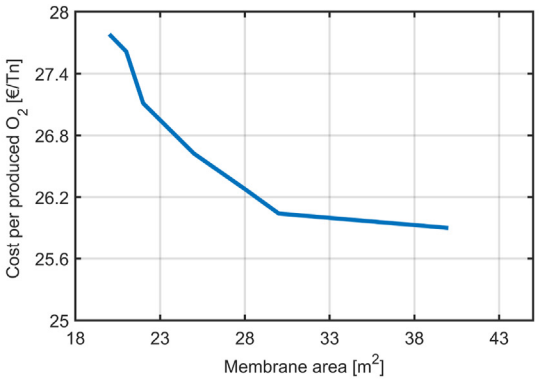

(b) Cost per produced oxygen variation respect to membrane area for Case 1.

Fig. 5. Oxygen production as a function of the membrane area for Case 1.

is an asymptotic behaviour. This is due to the effects of reducing the available energy in the turbines, causing a higher electric consumption, which is compensated with an increment in oxygen mass flow.

A similar performance is displayed in Case 2, as shown in Fig. 6a and Fig. 6b. It is seen that the same behaviour as Case 1 is performed, requiring smaller areas to produce oxygen. There is less available energy for the turbines due to a reduction in the oxygen-depleted mass flow increasing the electric energy consumption in HPEC and a higher requirement in the heat addition as a consequence of the same decrease in the oxygen-depleted mass flow, which reduces the heat transfer capacity in HE4.

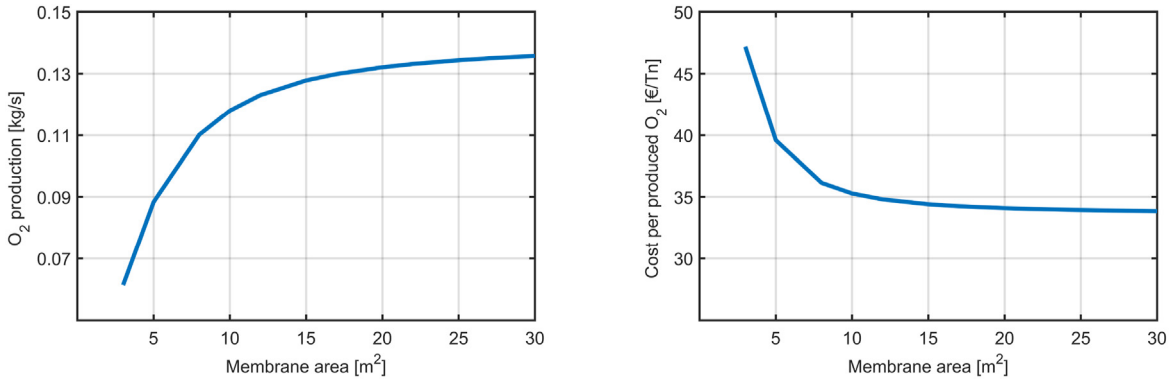

(a) Oxygen production variation respect to membrane area for Case 2.

(b) Cost per produced oxygen variation respect to membrane area for Case 2.

Fig. 6. Oxygen production as a function of the membrane area for Case 2.

In this case, a membrane area of 15 m^2 is selected, considering a higher availability of thermal energy in this case compared with Case 1, which is compensated with lower costs in facilities and maintenance by reducing the membrane area.

4.4. Variable geometry turbine nozzle positions

An optimisation process was performed for both cases, using the oxygen mass flow produced as the objective function during the calculation. The results are shown in Table 3. The efficiency of the turbomachines is kept high in all the cases but for the turbine that drives the O_2 compressor.

5. Performance evaluation and analysis

5.1. Case 1

A maximum value of oxygen mass flow of 0.124 kg s^{-1} is found at 75% of the maximum speed at HPEC and maximum speed at OLEC as it is depicted in Fig. 7a.

Higher OLEC speeds increase the oxygen mass flow due to a decrease in the vacuum pressure in the oxygen pipeline, which improves the membrane permeability. On the other hand, for the maximum value of OLEC speed, an optimum value of produced oxygen is achieved at 75% of the maximum HPEC speed.

As the HPEC speed increases, air mass flow and pressure increase, causing an improvement in the membrane performance because of a higher feed pressure. Nonetheless, there is a reduction in the membrane inlet temperature, as shown in Fig. 7b, due to a higher heat capacity in the air mass flow, decreasing the oxygen production as a result of declining O_2 permeation.

In Fig. 7c, as well as in FIgure 7d, it is noted that higher oxygen productions lead to an increase in the oxygen cost compared with the optimum cost point. The higher oxygen productions are achieved at high speeds in both electric compressors, increasing the pressure gradient at the membrane. Nonetheless, there is a reduction in the air temperature at the membrane inlet due to an increase in air heat capacity, affecting production. For lower speeds in both electric compressors, the pressure gradient is affected. However, a considerable increase in the air temperature at the membrane inlet is obtained, as it is seen in Fig. 7b due to a diminution in air heat capacity. Therefore, oxygen production at the optimum cost point is performed with low electric energy consumption and a high temperature but with less production because less air mass flow is driven through the membrane.

Likewise, it is shown that the cycle is cost-effective in the maximum production operation point, being 38% lower compared with the reference prices commonly available in the wholesale markets (50 €t^{-1}). Besides, these results show a certain level of flexibility during the operation of the cycle depending on the oxygen requirement in a particular moment, enhancing the production cost even if less oxygen is demanded. Therefore, the variation of the oxygen production as a function of the demand is pursued by driving the speeds through the gradient line between the maximum production point and smaller cost per produced oxygen (lower oxygen production) to operate with a better unitary cost under intermediate demand values.

Table 3
Optimum turbine nozzle positions and efficiencies for both cases.

Case	Turbocharger	Turbine position [%]	Turbine efficiency [%]	Compressor efficiency [%]	Speed [rpm]
1	Low pressure	20	75	74	50000
	Medium pressure	20	77	72	91000
	High pressure	16	59	74	59000
2	Low pressure	20	66	72	30000
	Medium pressure	20	73	71	61000
	High pressure	15	67	74	88000
	O_2 line	80	36	72	102000

5.2. Case 2

As the heater assures the MIEC inlet temperature at the end of the heat recovery stages, Fig. 8a depicts a high dependence in the HPEC speed to cause an increment in oxygen production. In this case, it should be clarified that opening percentages for the wastegate (WG0 at Fig. 2) higher than 20% are considered to avoid cycle instabilities, especially under low compressor speeds.

Higher HPEC speeds imply an increase in the MIEC pressure inlet, which improves the oxygen production. The maximum oxygen production is found at the maximum speed of the HPEC and a 30% of wastegate opening, achieving 0.227 kg s^{-1} of oxygen production. Nonetheless, there is also an increase in the air mass flow, leading to a decrease in the temperature after the heat recovery stages. For this reason, considering a lower temperature before the heater and a higher air mass flow, the required thermal energy rises.

Given the above, Fig. 8b depicts the cost per produced oxygen during the operation of Case 2. It is observed how the highest HPEC

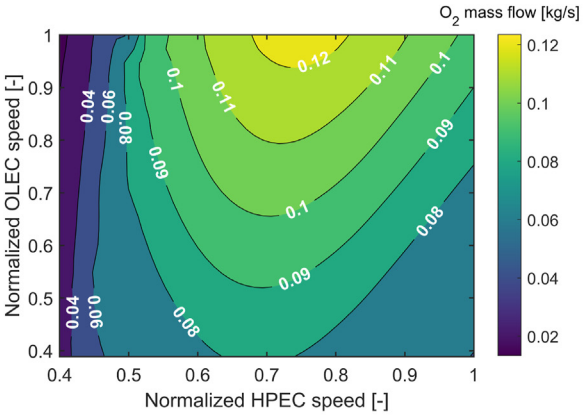

(a) O_2 mass flow as a function of both electric compressor speeds in Case 1.

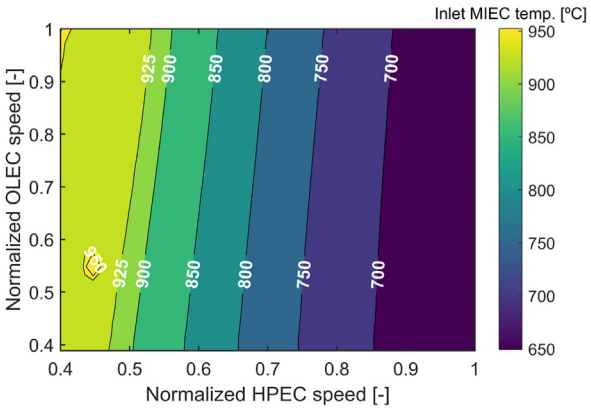

(b) MIEC inlet temperature as a function of both electric compressor speeds in Case 1.

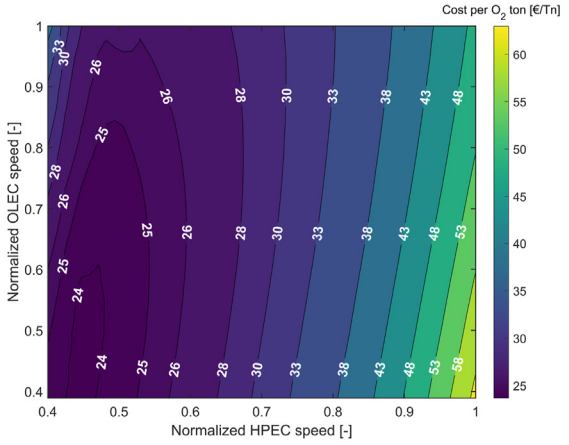

(c) Cost per mass of O_2 produced as a function of both electric compressor speeds in Case 1.

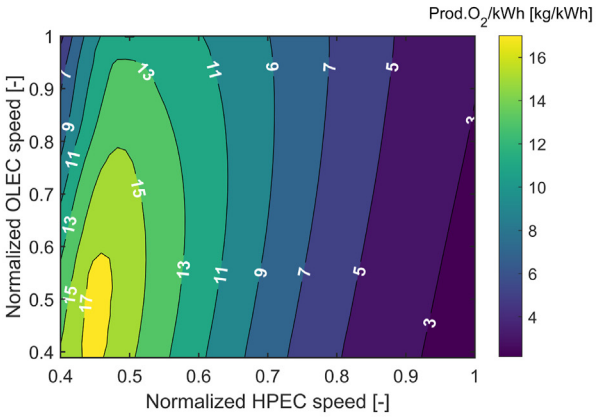

(d) Produced O_2 per kW h as function of electric compressor speeds in Case 1.

Fig. 7. O_2 production as a function of the electric compressor speeds in Case 1.

speeds lead to an increase in electric and thermal energy consumption due to an increased air mass flow, as it was explained. It is shown that, compared with the 50 €t^{-1} value taken as a market reference, the use of this configuration is profitable running the HPEC under 71%–85% of the maximum speed, depending on the wastegate opening, which implies less thermal energy addition at the heater.

Considering the latter, Fig. 8a indicates acceptable values of oxygen production under 60% of the maximum speed of HPEC, achieving 0.12 kg s^{-1}, which is initially proposed in the cycle description.

In this regard, lower HPEC speeds decrease both air mass flow and pressure at the membrane inlet, reducing oxygen production. However, the energy consumption, thermal and electric, is reduced: first, less thermal energy is required because a reduced air mass flow with a higher temperature reaches the heater inlet, and the electric power is diminished due to the reduced speed. This improves the energy consumption as it is seen in Fig. 8c.

6. Discussion

The different cycle components are selected for two cases where a heat exchanger (HE3 in Case 1, HE4 in Case 2) is identified as a critical component during operation, as it is directly coupled with the inlet flow at the expansion stages. This makes this heat exchanger to affect both electric and thermal consumption.

For Case 1, it is important to remark the importance of HE4, where flue gases from the plant contribute to the air heating before the membrane, being this the primary source of thermal energy for this scenario. Similarly two optimum operation points have been identified: maximum production and other of minimum production cost. Thus, it is recommended, for intermediate operation points (between 0.06 kg s^{-1} to 0.1235 kg s^{-1}), to operate in conditions whose production cost is minimum, which are obtained by using optimisation methods. Regarding profitability, the maximum production point exhibits a production cost of 30.8 €t^{-1}, which is 38% smaller than the current average cost available in the wholesale markets, being a feasible option to implement in the ceramic industry.

For Case 2, it should be mentioned as a critical component the turbocharger T0-C0, that restricts the available energy in the medium and low-pressure turbines, affecting the electric energy consumption and the membrane inlet pressure. This also occurs due to mass flow disequilibrium between the turbine and the compressor, causing a considerable energy loss in this component. Regarding the maximum oxygen mass flow produced, in this particular case the cycle can generate amounts as high as 0.227 kg s^{-1}, being almost twice the proposed production in the

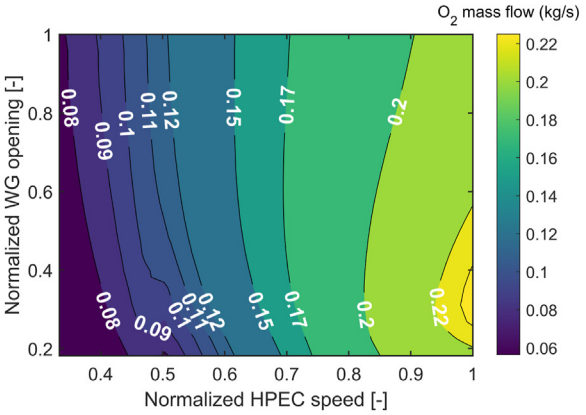

(a) O_2 mass flow as a function of electric compressor speed and wastegate opening in Case 2.

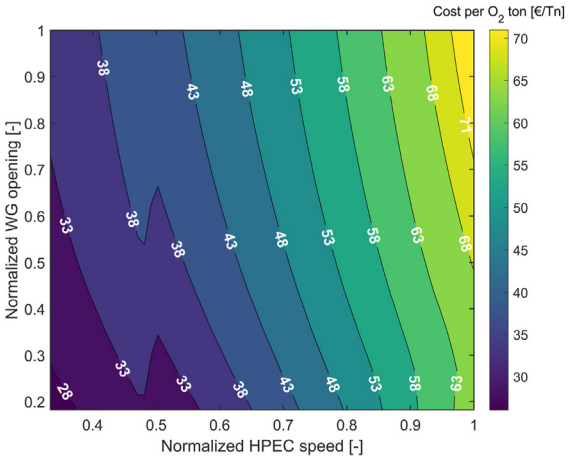

(b) Cost per O_2 mass produced as a function of electric compressor speed and waste gate opening in Case 2.

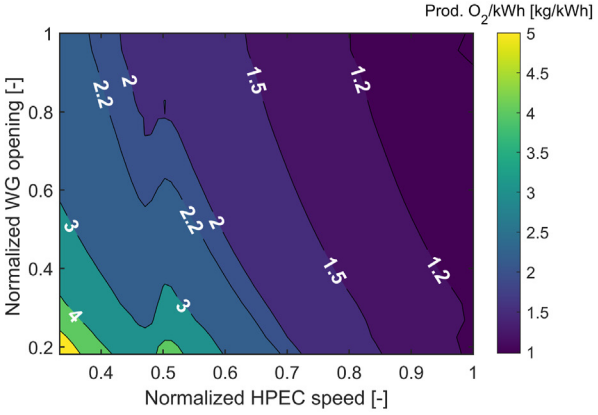

(c) Produced O_2 per kW h as a function of electric compressor speed and waste gate opening in Case 2.

Fig. 8. O_2 production as a function of the electric compressor speed and waste gate opening in Case 2.

initial description of this cycle. However, this production has a cost of 65.4 €t^{-1}, which exceeds in 30% the current available price in the wholesale market. Consequently, the cost for the maximum oxygen flow is not profitable.

Therefore, if a competitive cost with an acceptable production, Case 2 must operate in the region of Fig. 8b whose values in the production costs are less than 50 €t^{-1}, being the maximum production of 0.18 kg s^{-1} under this restriction. This is accomplished under HPEC speeds that range between 70% and 85% of its maximum, being highly dependent on the WG valve opening. A critical value is not exhibited regarding the production cost itself. However, taking as a reference a production of 0.12 kg s^{-1}, a cost production between 33 €t^{-1} to 38 €t^{-1} is estimated, being this 20%–30% smaller than the available price in the wholesale market.

Given the above, comparing both cases of the presented cycle, it is demonstrated that Case 2 has a higher oxygen production, which is a result of its high thermal energy consumption to guarantee a temperature of 1000 °C at the entrance of the membrane. Nonetheless, this consumption limits the operative range for this case, where a considerable part of the studied operation points is not profitable compared with the average oxygen cost in the market.

The latter contrasts with Case 1, where oxygen production levels are smaller but the profitability in the different operation points studied limits the operation only for high speeds in HPEC and medium to low speeds in OLEC. In these conditions, a considerable air mass flow is driven through the cycle with a high inlet pressure in the membrane but a high vacuum pressure and low temperature. This leads to smaller oxygen production rates with high energy consumption.

Thus, both cycles can be implemented depending on the specific requirements and conditions of the user. When higher levels of oxygen production are required, trading off in a certain way the production cost, Case 2 could be implemented. Furthermore, when there is a lower demand of oxygen and the price is a more critical variable, Case 1 is shown as an acceptable option to be considered.

The discussion of the different prices in both cases can be extended by remarking that one of the reasons that leads to a smaller production cost in Case 1 is the better use of energy to generate the vacuum. In Fig. 9a, it is depicted the global efficiency of the turbocharger associated with the oxygen line in Case 2. It is shown a low efficiency in all the studied operation points, with a maximum value of 30%. Meanwhile, Fig. 9b depicts the variation of the compressor efficiency at the oxygen line in Case 1. It is shown that there is an average efficiency higher than 60%, with points

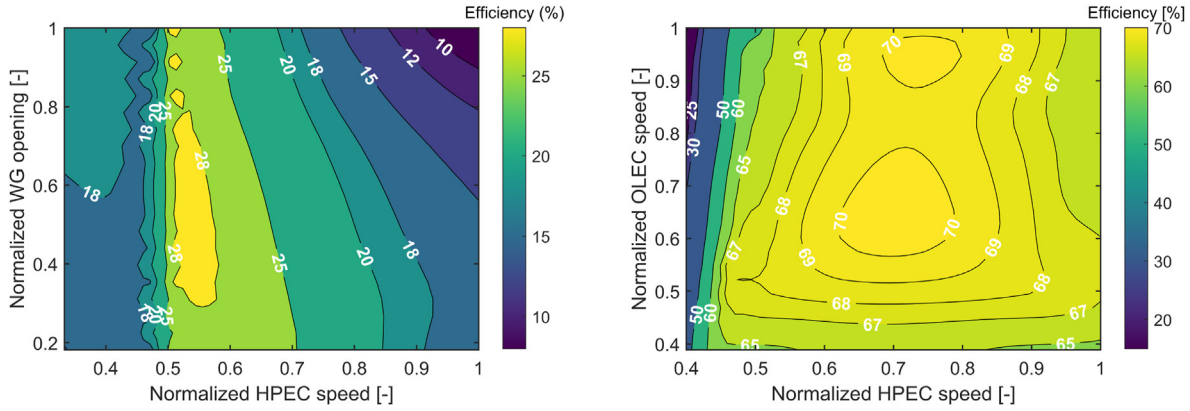

(a) Global efficiency of the turbocharger 0 as a function of controllable variables (Case 2).

(b) Efficiency of OLEC as a function of controllable variables (Case 1).

Fig. 9. Efficiency of turbocharger 0 in Case 2 and C0 in Case 1.

reaching an efficiency of 70% near the point of maximum production. This misused energy at Case 2 must be compensated with electric energy consumption at the HPEC to drive air mass flow and increase its pressure.

It should be mentioned also that, although the current calculations can be numerically stable, they may lead to extremely small surge margins in the OLEC in Case 1, specially in HPEC low speeds. Special attention must be given to these operation points, where scaling the current compressor or making a new selection are shown as the best alternatives to enhance the performed study.

On the other hand, an energy consumption comparison should be performed considering different oxygen production methods and their specific oxygen production. Table 4 exhibits different studies that have been performed applying the three leading technologies currently being developed for oxygen production.

Purity values in the produced oxygen stream are comparable with cryogenic methods, whose nature implies that other air components are dissolved in the oxygen stream, generating impurities in the production. On the other hand, compared with CLAS, Case 1 of the study seems to be price-competitive with the cited studies, reaching a higher purity due the exclusive oxygen permeation of the MIEC materials. However, higher production levels are reached in these studies, which could modify their specific production if similar oxygen production is demanded, as is also seen in this study.

7. Conclusions

An oxygen production plant using typical turbochargers from the automotive industry and heat recovery from flue gases from other processes near this facility is presented in this study. The designs of two cases of the O_2 production cycle are optimised where HE3 for Case 1 and HE4 for Case 2 are recognised as critical elements that affect both the electrical and thermal energy consumption, depending on the case. Additionally, HE4 for Case 1 and T0-C0 for Case 2 are identified as components that directly affect the performance of the cycle in both cases.

The behaviour of the cycle is assessed using indicators such as cost per mass of oxygen produced (€t^{-1}) and amount of oxygen per consumed energy (kg kW^{-1} h^{-1}). For Case 1, an optimum oxygen mass flow is found (0.1235 kg s^{-1}), reaching an acceptable production according to the oxygen production goal used in the initial steps of design. With a cost of 30.8/t, it is a competitive cycle when compared with wholesale market prices and an alternative to be applied in sectors where high purity oxygen is needed, such as the ceramic industry.

This optimum point of production is found in an equilibrium zone between high pressure and air mass flow at the membrane inlet and high temperature. Higher compressor speeds in HPEC generate lower temperatures at the membrane inlet while lower speeds lead to a smaller pressure gradient and air mass flow, affecting oxygen production.

The point of minimum cost is found in a zone of high temperature at the membrane inlet, facilitating oxygen production. Increasing the compressor speeds to increase the air mass flow and pressure gradient at the membrane denotes an increase in electric consumption proportionally higher than the increase in oxygen production, increasing its price. Regarding production per energy consumed, it has the same behaviour as the cost per production because electric energy is solely employed in this case.

For Case 2, an optimum point of oxygen production is found at HPEC maximum speed and a wastegate opening of 30% approximately, ensuring a considerable pressure gradient inside the membrane and high air mass flows. Nevertheless, it represents a cost of 61 €t^{-1}, which occurs due to the high thermal energy consumption as a consequence of maintaining a temperature of 1000 °C at the membrane inlet. Meanwhile, an optimum cost per oxygen production and oxygen produced per energy consumed is not found for the studied limits. However, for a production of 0.12 kg s^{-1}, a range of 33 €t^{-1} to 38 €t^{-1} is found, being profitable compared with the average wholesale market price.

Likewise, the operative feasibility of the cycle from an economic perspective is performed, identifying operation zones where the cost is lower than 50 €t^{-1}. For Case 1, it is found that the operation

Table 4
Comparing different oxygen production methods by their energy consumption.

Type	O_2 prod. [kg/kWh]	Purity [%]	O_2 flow [t h^{-1}]	Reference
Cryogenic	3.165	99.9	54.2	[50]
Cryogenic	2.915	99.6	142.9	[51]
CLAS	16.580	96.35	100	[52]
CLAS	8.906	30		[53]
CLAS	14.990	95	150	[54]
Adsorption	1.121	94	0.064	[55]
Adsorption	1.374	95	0.137	[56]
This study (Case 1)	8.000–17.000	100	0.214–0.445	
This study (Case 2)	1.200–2.800	100	0.432–0.817	

points where the HPEC speed is lower than 95% of its maximum speed belong to the competitive zone with respect to the wholesale market price. Also, for Case 2, a competitive zone is found for a HPEC lower than 85% of its maximum speed, exhibiting a higher dependence of the waste gate valve opening that controls the T0 mass flow. The production levels for Case 1 are lower than Case 2, while it is more profitable. Thus, depending on the availability of energy resources and the oxygen requirements, it is observed that both cases could be applied for applications like ceramic plants, showing acceptable profitability in a wide range of operation points of the cycle.

When comparing this oxygen production cycle using MIEC membranes with other methods in the literature, it is shown as a price-competitive alternative when compared with the most promising method in development as it is CLAS. Additionally, the cycle produces an oxygen stream with higher purity than the most reliable method nowadays as it is CAS due the nature of the MIEC materials with a perfect selectivity for oxygen.

Declaration of competing interest

The authors declare that they have no known competing financial interests or personal relationships that could have appeared to influence the work reported in this paper.

Acknowledgment

This research work has been supported by Grant PDC2021-120821-I00 funded by MCIN/AEI/10.13039/501100011033 and by European Union NextGenerationEU/PRTR. This work has also been supported by Grant UPV-SOLGEN-79674 funded by the Vicerrectorado de Investigación de la Universitat Politècnica de València (PAID-11-21). The authors want to acknowledge the institution "Conselleria d'Educació, Investigació, Cultura i Esport de la Generalitat Valenciana" and its grant program "Subvenciones para la contratación de personal investigador de carácter predoctoral" for doctoral studies (ACIF/2020/246) funded by The European Union. Also, this work is part of grant number INNVA1/2021/38 funded by "Agencia Valenciana de la Innovación (AVI)" and by "ERDF A way of making Europe".

Appendix A. Scaled compressor maps

Figure A.10 to Figure A.16 show the compressor maps used in this work. In these figures, the corrected mass flow $\dot{m}^*$ is defined in Equation A.1, the compression ratio π_{comp} is defined in Equation A.2, the corrected speed is defined in Equation A.3 and the compressor adiabatic efficiency is defined in Equation A.4. In these equations, $p_{2,t}$ is the compressor outlet total pressure, p_{ref} is a reference pressure equal to 101 325 Pa, T_{ref} is a reference temperature equal to 288.15 K, $\dot{W}$ is the compressor power, and $\dot{W}_s$ is the compressor isentropic power.

$$\dot{m}^* = \dot{m} \cdot \sqrt{\frac{T_{1,t}}{T_{ref}}} \cdot \frac{p_{ref}}{p_{1,t}} \tag{A.1}$$

$$\pi_{comp} = \frac{p_{2,t}}{p_{1,t}} \tag{A.2}$$

$$N^* = N \cdot \sqrt{\frac{T_{ref}}{T_{1,t}}} \tag{A.3}$$

$$\eta_{comp} = \frac{\dot{W}}{\dot{W}_s} \simeq \frac{T_{2,t} - T_{1,t}}{T_{1,t} \cdot \left(\pi_{comp}^{\frac{\gamma-1}{\gamma}} - 1 \right)} \tag{A.4}$$

A.1. Case 1

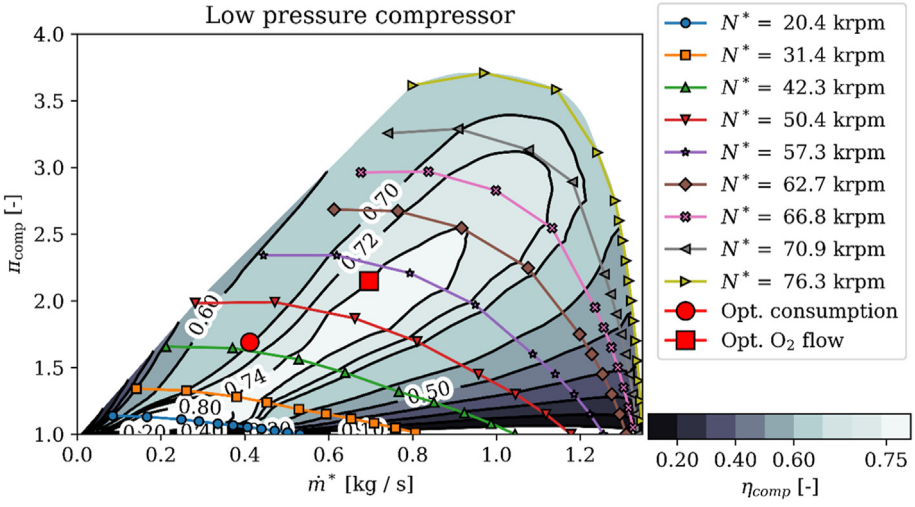

Fig. A.10. Low pressure compressor map in Case 1.

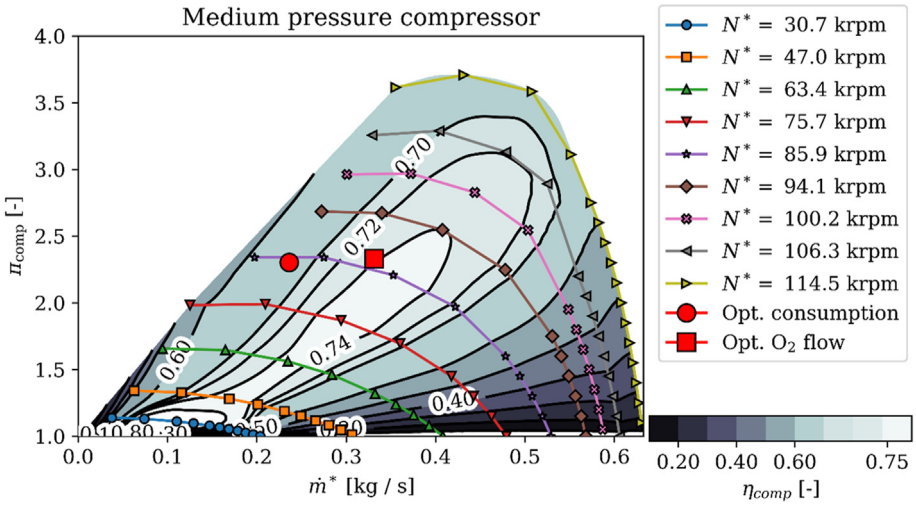

Fig. A.11. Medium pressure compressor map in Case 1.

A.2. Case 2

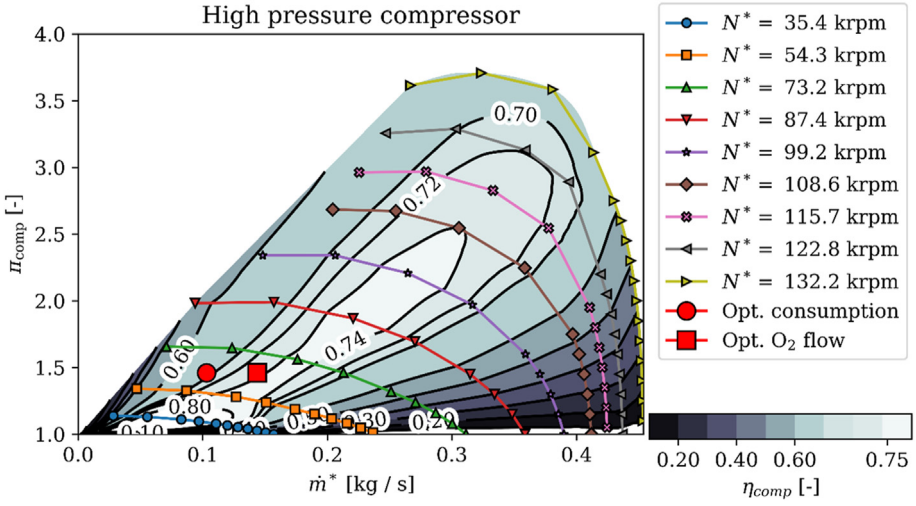

Fig. A.12. High pressure compressor map in Case 1.

Appendix B. Thermodynamic data of the cycle

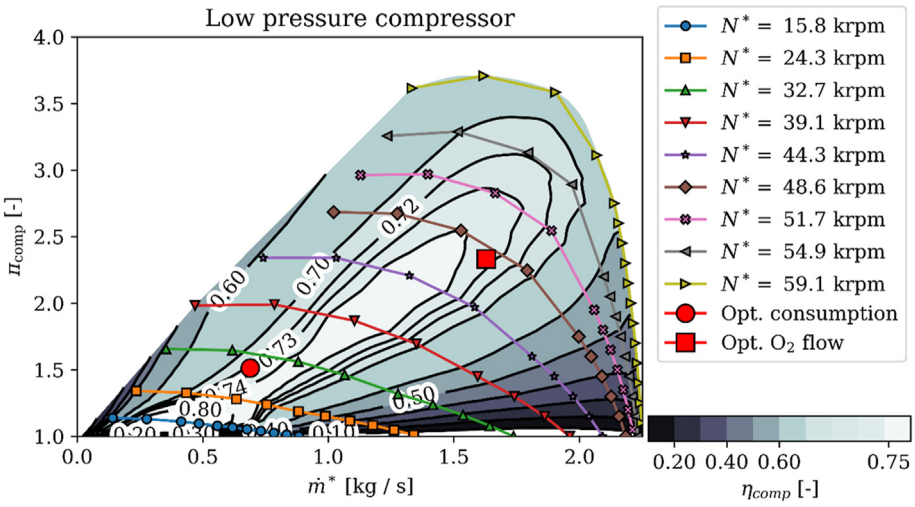

Fig. A.13. Low pressure compressor map in Case 2.

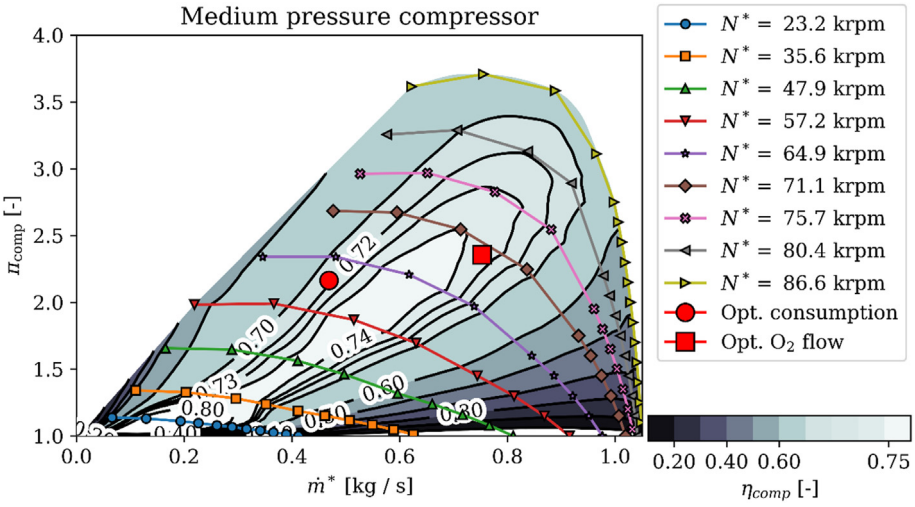

Fig. A.14. Medium pressure compressor map in Case 2.

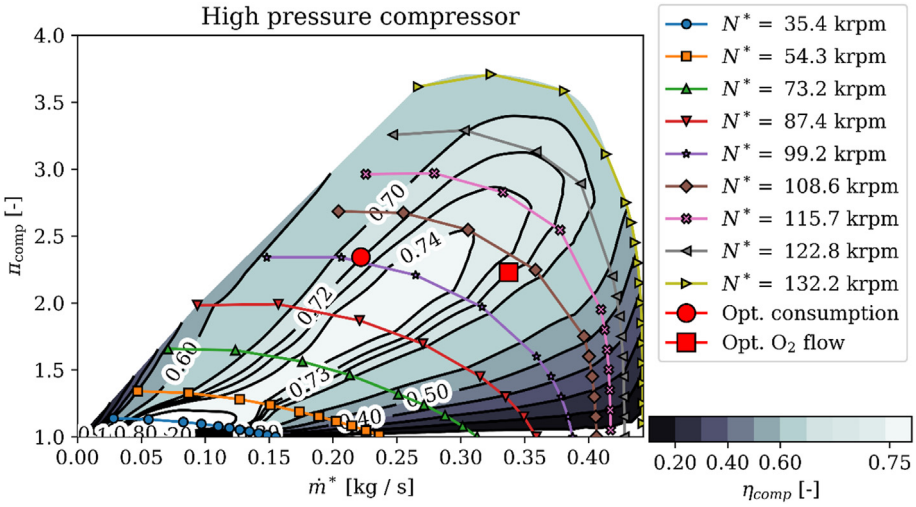

Fig. A.15. High pressure compressor map in Case 2.

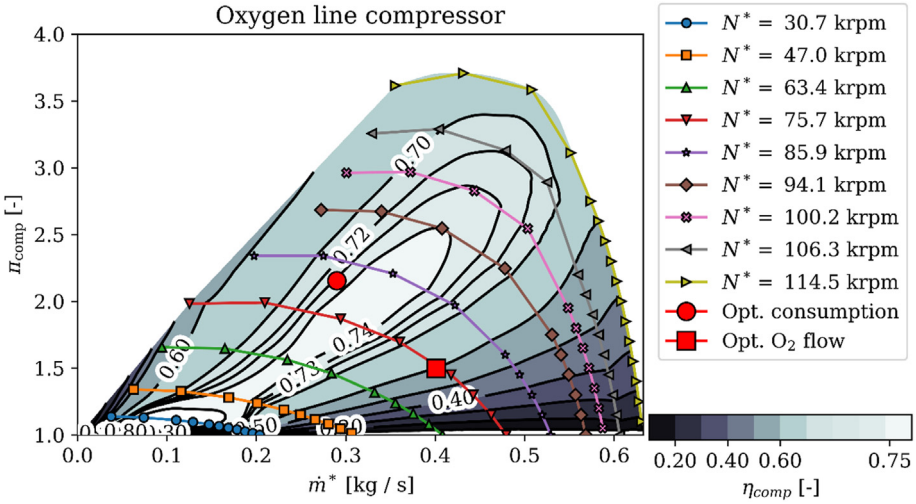

Fig. A.16. O_2 line compressor map in Case 2.

List of symbols

AEP	Average electricity price

ANP Average natural gas price

Table B.5
Thermodynamic data for the optimum mass flow point of Case 1.

Point	p [MPa]	T [K]	$\dot{m}$ [kg s^{-1}]
Low pressure air compressor inlet	0.100	25	0.726
Low pressure air compressor outlet	0.214	122	0.726
Medium pressure air compressor inlet	0.210	25	0.726
Medium pressure compressor air outlet	0.489	135	0.726
High pressure air compressor inlet	0.484	25	0.726
High pressure compressor air outlet	0.683	68	0.726
High pressure electric air compressor outlet	0.993	122	0.726
HE2′ air outlet	0.986	151	0.726
HE1 air outlet	0.979	228	0.726
HE2 air outlet	0.970	309	0.726
HE3 air outlet	0.966	528	0.726
HE4 air outlet	0.958	768	0.726
HE3 oxygen depleted inlet	0.957	768	0.603
High pressure turbine oxygen depleted inlet	0.956	524	0.603
Medium pressure turbine oxygen depleted inlet	0.643	478	0.603
Low pressure turbine oxygen depleted inlet	0.261	366	0.603
HE3 oxygen depleted inlet	0.101	261	0.603
HE3 oxygen depleted outlet	0.101	171	0.603
HE2 oxygen inlet	0.044	769	0.124
HE2′ oxygen inlet	0.044	313	0.124
Intercooling inlet	0.043	153	0.124
Oxygen line electric compressor inlet	0.039	50	0.124
Oxygen line electric compressor outlet	0.1	185	0.124

C1 Low pressure compressor

Table B.6
Thermodynamic data for the optimum cost per kilogram point of Case 1.

Point	p [MPa]	T [K]	$\dot{m}$ [kg s^{-1}]
Low pressure air compressor inlet	0.100	25	0.445
Low pressure air compressor outlet	0.180	104	0.445
Medium pressure air compressor inlet	0.178	25	0.445
Medium pressure compressor air outlet	0.414	144	0.445
High pressure air compressor inlet	0.411	25	0.445
High pressure compressor air outlet	0.601	76	0.445
High pressure electric air compressor outlet	0.679	99	0.445
HE2′ air outlet	0.675	138	0.445
HE1 air outlet	0.670	324	0.445
HE2 air outlet	0.665	394	0.445
HE3 air outlet	0.662	665	0.445
HE4 air outlet	0.657	943	0.445
HE3 oxygen depleted inlet	0.	768	0.386
High pressure turbine oxygen depleted inlet	0.956	524	0.386
Medium pressure turbine oxygen depleted inlet	0.643	478	0.386
Low pressure turbine oxygen depleted inlet	0.261	366	0.386
HE1 oxygen depleted inlet	0.101	261	0.386
HE1 oxygen depleted outlet	0.101	171	0.386
HE2 oxygen inlet	0.080	943	0.059
HE2′ oxygen inlet	0.080	419	0.059
Intercooling inlet	0.080	151	0.059
Oxygen line electric compressor inlet	0.079	50	0.059
Oxygen line electric compressor outlet	0.1	86	0.059

C2 Medium pressure compressor

Table B.7
Thermodynamic data for the optimum mass flow point of Case 2.

Point	p [MPa]	T [K]	$\dot{m}$ [kg s^{-1}]
Low pressure air compressor inlet	0.100	25	1.690
Low pressure air compressor outlet	0.233	135	1.690
Medium pressure air compressor inlet	0.216	25	1.690
Medium pressure compressor air outlet	0.512	137	1.690
High pressure air compressor inlet	0.486	25	1.690
High pressure compressor air outlet	1.068	129	1.690
High pressure electric air compressor inlet	1.013	95	1.690
High pressure electric air compressor outlet	2.255	229	1.690
HE2′ air outlet	2.240	247	1.690
HE1 air outlet	2.214	296	1.690
HE2 air outlet	2.191	384	1.690
HE3 air outlet	2.176	501	1.690
HE4 air outlet	2.163	801	1.690
H1 air outlet	2.156	1000	1.690
HE3 oxygen depleted inlet	2.154	1000	1.415
High pressure turbine oxygen depleted inlet	2.073	654	1.415
High pressure turbine oxygen depleted outlet	0.952	555	1.415
Bypassed oxygen depleted flow	0.714	555	0.397
Turbine 0 oxygen depleted inlet	0.950	555	1.021
Turbine 0 oxygen depleted outlet	0.714	538	1.021
Medium pressure turbine oxygen depleted inlet	0.713	543	1.415
Low pressure turbine oxygen depleted inlet	0.290	433	1.415
HE1 oxygen depleted inlet	0.102	320	1.415
HE1 oxygen depleted outlet	0.101	262	1.415
Oxygen membrane outlet	0.084	1000	0.272
HE2 oxygen inlet	0.081	922	0.272
HE2′ oxygen inlet	0.081	387	0.272
Intercooling inlet	0.079	277	0.272
Oxygen line electric compressor inlet	0.065	50	0.272
Oxygen line electric compressor outlet	0.102	122	0.272

Table B.8
Thermodynamic data for the optimum cost per kilogram point of Case 2

Point	p [MPa]	T [K]	$\dot{m}$ [kg s^{-1}]
Low pressure air compressor inlet	0.100	25	0.726
Low pressure air compressor outlet	0.152	79	0.726
Medium pressure air compressor inlet	0.147	25	0.726
Medium pressure compressor air outlet	0.319	128	0.726
High pressure air compressor inlet	0.312	25	0.726
High pressure compressor air outlet	0.731	139	0.726
High pressure electric air compressor inlet	0.716	95	0.726
High pressure electric air compressor outlet	1.011	149	0.726
HE2′ air outlet	1.006	193	0.726
HE1 air outlet	0.995	382	0.726
HE2 air outlet	0.984	467	0.726
HE3 air outlet	0.976	697	0.726
HE4 air outlet	0.970	873	0.726
H1 air outlet	0.967	1000	0.726
HE3 oxygen depleted inlet	2.154	1000	0.589
High pressure turbine oxygen depleted inlet	2.073	654	0.589
High pressure turbine oxygen depleted outlet	0.952	555	0.589
Bypassed oxygen depleted flow	0.714	555	0.119
Turbine 0 oxygen depleted inlet	0.950	555	0.470
Turbine 0 oxygen depleted outlet	0.714	538	0.470
Medium pressure turbine oxygen depleted inlet	0.713	543	0.589
Low pressure turbine oxygen depleted inlet	0.290	433	0.589
HE1 oxygen depleted inlet	0.102	320	0.589
HE1 oxygen depleted outlet	0.101	262	0.589
Oxygen membrane outlet	0.084	1000	0.137
HE2 oxygen inlet	0.081	922	0.137
HE2′ oxygen inlet	0.081	387	0.137
Intercooling inlet	0.079	277	0.137
Oxygen line electric compressor inlet	0.065	50	0.137
Oxygen line electric compressor outlet	0.102	122	0.137

C3	High pressure compressor
CF	Conversion factor for natural gas
CAS	Cryogenic air separation
CLAS	Chemical looping air separation
D	Wheel diameter
η_{comp}	Compressor adiabatic efficiency
γ	Ratio of heat capacities
H1	Heater
HE1	Heat exchanger between compressed air and O_2 depleted air
HE2	First heat exchanger between air and O_2
HE2'	Second heat exchanger between air and O_2
HE3	Third heat exchanger
HE4	Fourth heat exchanger
HPEC	High pressure electric compressor
IC1	First air intercooler
IC2	Second air intercooler
IC O_2	O_2 line intercooler
$\dot{m}$	Mass flow rate
$\dot{m}^*$	Corrected mass flow
$\dot{m}$	Non-dimensional mass flow
$\dot{m}_{NG}$	Natural gas mass flow
MIEC	Mixed ionic-electronic conducting membrane
N	Rotational speed
N^*	Corrected rotational speed
$\tilde{N}$	Non-dimensional rotational speed
OLEC	O_2 line electric compressor
p	Pressure
p_{ref}	Reference pressure
$p_{1,t}$	Inlet total pressure
$p_{2,t}$	Outlet total pressure
π_{comp}	Total to total compression ratio
$\dot{Q}$	Heat
R	Gas constant
T1	Low pressure turbine
T2	Medium pressure turbine
T3	High pressure turbine
T	Temperature
T_{ref}	Reference temperature
$T_{1,t}$	Inlet total temperature
$T_{2,t}$	Outlet total temperature
$\dot{W}$	Power
$\dot{W}_s$	Isentropic power
WG	Waste gate

References

[1] Levi P, Vass T, Mandová H, Gouy A, Schröder A. Tracking industry. 2020. URL: https://www.iea.org/reports/tracking-industry-2020, visited on 2021-03-05.

[2] Energy Agency International. Emissions of Nitrogen oxyde (NOx) by sector and scenario, 2015 and 2040. 2019. URL: https://www.iea.org/data-and-statistics/charts/emissions-of-nitrogen-oxyde-nox-by-sector-and-scenario-2015-and-2040, visited on 2021-03-05.

[3] Koohestanian E, Shahraki F. Review on principles, recent progress, and future challenges for oxy-fuel combustion CO2 capture using compression and purification unit. J Environ Chem Eng 2021;9:105777. https://doi.org/10.1016/j.jece.2021.105777.

[4] Van Blarigan A, Kozarac D, Seiser R, Cattolica R, Chen J-Y, Dibble R. Experimental study of methane fuel oxycombustion in a spark-ignited engine. J Energy Resour Technol 2014;136:012203. https://doi.org/10.1115/1.4024974.

[5] Tan Q, Hu Y. A study on the combustion and emission performance of diesel engines under different proportions of O_2 & N_2 & CO_2. Appl Therm Eng 2016;108:508–15. https://doi.org/10.1016/j.applthermaleng.2016.07.151.

[6] Wu Z, Fu L, Gao Y, Yu X, Deng J, Li L. Thermal efficiency boundary analysis of an internal combustion Rankine cycle engine. Energy 2016;94:38–49. https://doi.org/10.1016/j.energy.2015.10.099.

[7] Kang Z, Wu Z, Zhang Z, Deng J, Hu Z, Li L. Study of the combustion characteristics of a HCCI engine coupled with oxy-fuel combustion mode. SAE Int. J. Engine. 2017;10. https://doi.org/10.4271/2017-01-0649.

[8] Thorbergsson E, Grönstedt T. A thermodynamic analysis of two competing mid-sized oxyfuel combustion combined cycles. J Energy 2016;2016. https://doi.org/10.1155/2016/2438431.

[9] Hanak DP, Powell D, Manovic V. Techno-economic analysis of oxy-combustion coal-fired power plant with cryogenic oxygen storage. Appl Energy 2017;191:193–203. https://doi.org/10.1016/j.apenergy.2017.01.049.

[10] Park SK, Kim TS, Sohn JL, Lee YD. An integrated power generation system combining solid oxide fuel cell and oxy-fuel combustion for high performance and CO_2 capture. Appl Energy 2011;88:1187–96. https://doi.org/10.1016/j.apenergy.2010.10.037.

[11] Carrasco-Maldonado F, Spörl R, Fleiger K, Hoenig V, Maier J, Scheffknecht G. Oxy-fuel combustion technology for cement production – state of the art research and technology development. Int J Greenh Gas Control 2016;45:189–99. https://doi.org/10.1016/j.ijggc.2015.12.014.

[12] Escudero AI, Espatolero S, Romeo LM. Oxy-combustion power plant integration in an oil refinery to reduce CO_2 emissions. Int J Greenh Gas Control 2016;45:118–29. https://doi.org/10.1016/j.ijggc.2015.12.018.

[13] Anderson R, Hustad C, Skutley P, Hollis R. Oxy-fuel turbo machinery development for energy intensive industrial applications. Energy Proc 2014;63:511–23. https://doi.org/10.1016/j.egypro.2014.11.056. 12th International Conference on Greenhouse Gas Control Technologies, GHGT-12.

[14] Li C, Chew JJ, Mahmoud A, Liu S, Sunarso J. Modelling of oxygen transport through mixed ionic-electronic conducting (MIEC) ceramic-based membranes: an overview. J Membr Sci 2018;567:228–60. https://doi.org/10.1016/j.memsci.2018.09.016.

[15] Cau G, Tola V, Ferrara F, Porcu A, Pettinau A. CO_2-free coal-fired power generation by partial oxy-fuel and post-combustion CO_2 capture: techno-economic analysis. Fuel 2018;214:423–35. https://doi.org/10.1016/j.fuel.2017.10.023.

[16] Xiong J, Zhao H, Zheng C. Exergy analysis of a 600 MWe oxy-combustion pulverized-coal-fired power plant. Energy Fuel. 2011;25:3854–64. https://doi.org/10.1021/ef200702k.

[17] Wu F, Argyle MD, Dellenback PA, Fan M. Progress in O_2 separation for oxy-fuel combustion–A promising way for cost-effective CO_2 capture: a review. Prog Energy Combust Sci 2018;67:188–205. https://doi.org/10.1016/j.pecs.2018.01.004.

[18] Simpson AP, Simon A. Second law comparison of oxy-fuel combustion and post-combustion carbon dioxide separation. Energy Convers Manag 2007;48:3034–45. https://doi.org/10.1016/j.enconman.2007.06.047,19th [International Conference on Efficiency, Cost, Optimization, Simulation and Environmental Impact of Energy Systems].

[19] Habib MA, Nemitallah M, Ben-Mansour R. Recent development in oxy-combustion technology and its applications to gas turbine combustors and ITM reactors. Energy Fuel. 2013;27:2–19. https://doi.org/10.1021/ef301266j.

[20] Zhu Yu, Liu Xinggao, Zhou Zhiyong. Optimization of cryogenic air separation distillation columns. In: 2006 6th world congress on intelligent control and automation, vol. 2; 2006. p. 7702–5. https://doi.org/10.1109/WCICA.2006.1713466.

[21] Yang R. Gas separation by adsorption processes. Butterworths; 1987.

[22] Smith A, Klosek J. A review of air separation technologies and their integration with energy conversion processes. Fuel Process Technol 2001;70:115–34. https://doi.org/10.1016/S0378-3820(01)00131-X.

[23] NZ Institute of Chemistry. Production of chemicals. 2018. visited on 2021-13-21, https://nzic.org.nz/chemical-processes-new-zealand/production-of-chemicals.

[24] C. Zhou, S. K, S. H, Z. J, D. E, M. B. Integration options and economic analysis of an integrated chemical looping air separation. Energy Fuels 2016. https://doi.org/10.1021/acs.energyfuels.5b02209.

[25] Shah K, Zhou C, Song H, Doroodchi E, Moghtaderi B. Integration options and economic analysis of an integrated chemical looping air separation. Energy Fuels 2016. https://doi.org/10.1021/acs.energyfuels.5b02209.

[26] Zhu X, Yang W. Mixed conducting ceramic membranes fundamentals, materials and applications. Springer; 2017.

[27] Arratibel Plazaola A, Cruellas Labella A, Liu Y, Badiola Porras N, Pacheco Tanaka DA, Sint Annaland MV, Gallucci F. Mixed ionic-electronic conducting membranes (MIEC) for their application in membrane reactors. Rev. Proc. 2019;7. https://doi.org/10.3390/pr7030128.

[28] Castillo R. Thermodynamic analysis of a hard coal oxyfuel power plant with high temperature three-end membrane for air separation. Appl Energy 2011;88:1480–93. https://doi.org/10.1016/j.apenergy.2010.10.044.

[29] Skorek-Osikowska A, Bartela Łukasz, Kotowicz J. A comparative thermodynamic, economic and risk analysis concerning implementation of oxy-combustion power plants integrated with cryogenic and hybrid air separation units. Energy Convers Manag 2015;92:421–30. https://doi.org/10.1016/j.enconman.2014.12.079.

[30] Portillo E, Gallego-Fernandez LM, Vega F, Alonso-Farinas B, Navarrete B. Oxygen transport membrane unit applied to oxy-combustion coal power plants: a thermodynamic assessment. J Environ Chem Eng 2021;9:105266. https://doi.org/10.1016/j.jece.2021.105266.

[31] Anderson LL, Armstrong PA, Broekhuis RR, Carolan MF, Chen J, Hutcheon MD, Lewinsohn CA, Miller CF, Repasky JM, Taylor DM, Woods CM. Advances in ion transport membrane technology for oxygen and syngas production. Solid State Ionics 2016;288:331–7. https://doi.org/10.1016/j.ssi.2015.11.010. proceedings of the 20th International Conference on Solid State Ionics SSI-20.

[32] Technology Inc Praxair. Composite oxygen transport membrane. US patent US20130156978A1; 2014.
[33] Technology Inc Praxair, BP Corp North America Inc. Syngas production utilizing an oxygen transport membrane. US patent US6695983B2; 2004.
[34] Technology Inc Praxair. Oxygen transport membrane reactor based method and system for generating electric power. 2015. Canada patent CA2937943A1.
[35] Bai W, Feng J, Luo C, Zhang P, Wang H, Yang Y, Zhao Y, Fan H. A comprehensive review on oxygen transport membranes: development history, current status, and future directions. Int J Hydrogen Energy 2021;46:36257–90. https://doi.org/10.1016/j.ijhydene.2021.08.177.
[36] Zhu X, Sun S, Cong Y, Yang W. Operation of perovskite membrane under vacuum and elevated pressures for high-purity oxygen production. J Membr Sci 2009;345:47–52. https://doi.org/10.1016/j.memsci.2009.08.020.
[37] Martin J, Arnau F, Piqueras P, Auñón A. Development of an integrated virtual engine model to simulate new standard testing cycles. In: WCX world congress experience, SAE International; 2018. https://doi.org/10.4271/2018-01-1413.
[38] Catalán-Martínez D, Santafé-Moros A, Gozálvez-Zafrilla J, García-Fayos J, Serra J. Characterization of oxygen transport phenomena on BSCF membranes assisted by fluid dynamic simulations including surface exchange. Chem Eng J 2020;387:124069. https://doi.org/10.1016/j.cej.2020.124069.
[39] Serrano JR, Olmeda P, Tiseira A, García-Cuevas LM, Lefebvre A. Theoretical and experimental study of mechanical losses in automotive turbochargers. Energy 2013;55:888–98. https://doi.org/10.1016/j.energy.2013.04.042.
[40] Serrano JR, Olmeda P, Arnau FJ, Reyes-Belmonte MA, Tartoussi H. A study on the internal convection in small turbochargers. proposal of heat transfer convective coefficients. Appl Therm Eng 2015;89:587–99. https://doi.org/10.1016/j.applthermaleng.2015.06.053.
[41] Serrano JR, Olmeda P, Arnau FJ, Dombrovsky A. General procedure for the determination of heat transfer properties in small automotive turbochargers. SAE Int. J. Engine. 2015;8:30–41. https://doi.org/10.4271/2014-01-2857.
[42] Serrano JR, Olmeda P, Arnau FJ, Dombrovsky A, Smith L. Methodology to characterize heat transfer phenomena in small automotive turbochargers: experiments and modelling based analysis. In: Proceedings of the ASME turbo expo 2014: turbine technical conference and exposition, volume 1B: marine; microturbines, turbochargers and small turbomachines. Steam Turbines, ASME; 2014. https://doi.org/10.1115/GT2014-25179. paper No: GT2014-25179.
[43] Serrano J, Arnau F, Dolz V, Tiseira A, Cervelló C. A model of turbocharger radial turbines appropriate to be used in zero- and one-dimensional gas dynamics codes for internal combustion engines modelling. Energy Convers Manag 2008;49:3729–45. https://doi.org/10.1016/j.enconman.2008.06.031.
[44] Payri F, Serrano J, Fajardo P, Reyes-Belmonte M, Gozalbo-Belles R. A physically based methodology to extrapolate performance maps of radial turbines. Energy Convers Manag 2012;55:149–63. https://doi.org/10.1016/j.enconman.2011.11.003.
[45] Galindo J, Navarro R, García-Cuevas LM, Tarí D, Tartoussi H, Guilain S. A zonal approach for estimating pressure ratio at compressor extreme off-design conditions. Int J Engine Res 2019;20:393–404. https://doi.org/10.1177/1468087418754899.
[46] Galindo J, Tiseira A, Navarro R, Tarí D, Tartoussi H, Guilain S. Compressor efficiency extrapolation for 0D-1D engine simulations. In: SAE 2016 world congress and exhibition. SAE International; 2016. https://doi.org/10.4271/2016-01-0554.
[47] Park C, Ebisu M, Bae C. Effects of turbocharger rotational inertia on engine and turbine performance in a turbocharged gasoline direct injection engine under transient and steady conditions. Int J Engine Res 2021. https://doi.org/10.1177/1468087420984600. published in OnlineFirst.
[48] Shubnikova E, Popov M, Bychkov S, Chizhik S, Nemudry A. The modeling of oxygen transport in miec oxide hollow fiber membranes. Chem Eng J 2019;372:251–9. https://doi.org/10.1016/j.cej.2019.04.126.
[49] Li C, Li W, Chew JJ, Liu S, Zhu X, Sunarso J. Oxygen permeation through single-phase perovskite membrane: modeling study and comparison with the dual-phase membrane. Separ Purif Technol 2020;235:116224. https://doi.org/10.1016/j.seppur.2019.116224.
[50] Aneke M, Wang M. Potential for improving the energy efficiency of cryogenic airseparation unit (asu) using binary heat recovery cycles. Applied Thermal Engineering; 2015. https://doi.org/10.1016/j.applthermaleng.2015.02.034.
[51] Xu J, Wang T, Chen Q, Zhang S, Tan J. Performance design of a cryogenic air separation unit for variable working conditions using the lumped parameter model. Front Mech Eng 2020. https://doi.org/10.1016/j.energy.2019.116579.
[52] Cormos C-C. Energy and cost efficient manganese chemical looping air separationcycle for decarbonized power generation based on oxy-fuelcombustion and gasification. Energy; 2020. https://doi.org/10.1007/s11465-019-0558-6.
[53] Qing M, Jin B, Ma J, Zou X, Wang X, Zheng C, Zhao H. Thermodynamic and economic performance of oxy-combustionpower plants integrating chemical looping air separation. Energy; 2020. https://doi.org/10.1016/j.energy.2020.117876.
[54] Zhang D, Duan R, Li H, Yang Q, Zhou H. Optimal design, thermodynamic, cost and co2emission analyses ofcoal-to-methanol process integrated with chemical looping airseparation and hydrogen technology. Energy; 2020. https://doi.org/10.1016/j.energy.2020.117876.
[55] Banaszkiewicz T, Chorowski M. Energy consumption of air-separation adsorption methods. Entropy 2018. https://doi.org/10.3390/e20040232.
[56] Šulc R, Ditl P. The potential of energy savings in oxygen production by pressure swing adsorption. Chem. Eng. Transact. 2021. https://doi.org/10.3303/CET2186053.